TRES_A_541506

International Journal of Remote Sensing
Vol. 32, No. 11, 10 June 2011, 1–14

Taylor & Francis
Taylor & Francis Group

Model of electronic-vibrational kinetics of the O_3 and O_2 photolysis products in the middle atmosphere: applications to water vapour retrievals from SABER/TIMED 6.3 μm radiance measurements

VALENTINE YANKOVSKY*†, RADA MANUILOVA†, ALEXANDER BABAEV†, ARTEM FEOFILOV‡§ and ALEXANDER KUTEPOV‡§

†Institute of Physics, St. Petersburg State University, 198504, Russia
‡The Catholic University of America, 620 Michigan Avenue, Washington DC 20064, USA
§NASA Goddard Space Flight Center, Mailcode 674, Greenbelt Road, Greenbelt, MD 20771, USA

In this work, we present a methodology of simple yet accurate calculations of $H_2O(v_2)$ vibrational levels pumping from the collisions with vibrationally excited $O_2(X^3\Sigma^-_g, v = 1)$ molecules, which is required for correct retrievals of H_2O volume mixing ratios from the 6.3 μm band radiance. The electronic-vibrational kinetics model of O_2 and O_3 photolysis products used in this study includes 44 electronic-vibrational states of the O_2 molecule (three states of $O_2(b^1\Sigma^+_g, v)$, six states of $O_2(a^1\Delta_g, v)$ and 35 states of $O_2(X^3\Sigma^-_g, v)$) as well as the first excited state of atomic oxygen, $O(^1D)$ and considers more than 100 photochemical reactions linking these states. We introduce the Resulting Quantum Output (RQO) approach that describes the $O_2(X^3\Sigma^-_g, v = 1)$ production quantum yield per one act of O_3 photolysis in the Hartley, Huggins, Chappuis and Wulf bands (200–900 nm). We demonstrate that the RQO weakly depends on latitude and season, and suggest a parameterization formula for the altitude dependence of this parameter. We show the application of RQO to H_2O retrievals from the 6.3 m broadband radiance measured by the Sounding of the Atmosphere using Broadband Emission Radiometry (SABER)/Thermosphere Ionosphere Mesosphere Energetics and Dynamics (TIMED) instrument that has been performing remote sensing of the Earth's atmosphere in the 13–110 km altitude range from 2002 onwards.

1. Introduction

This paper describes an important component required for the correct interpretation of 6.3 μm water vapour radiance in the mesosphere and lower thermosphere (MLT), the region that remains the least explored part of the Earth's atmosphere. This area is sensitive both to external influences from the Sun and to radiative transfer from the lower atmosphere, and is therefore considered to be an 'early warning system' for global changes in atmosphere. Water vapour is one of the key components of the middle atmosphere that influences the composition and energy budget of this region (Brasseur and Solomon 2005, Sonnemann *et al*. 2005). An adequate interpretation of H_2O infrared measurements requires an exact knowledge of all processes populating and depopulating the $H_2O(v_2)$ vibrational states. Among these processes, the

*Corresponding author. Email: vyankovsky@gmail.com

International Journal of Remote Sensing
ISSN 0143-1161 print/ISSN 1366-5901 online © 2011 Taylor & Francis
http://www.tandf.co.uk/journals
DOI: 10.1080/01431161.2010.541506

interaction with the first vibrationally excited state of $O_2(X)$ molecule plays a crucial role (López-Puertas and Taylor 2001, Manuilova *et al*. 2001, Feofilov *et al*. 2009). Its population, in turn, depends on a complex set of O_2/O_3 photochemical processes. The molecular oxygen photolysis in the Schumann–Runge continuum leads to formation of two oxygen atoms: one in the ground electronic state $O(^3P)$, and another one in the excited electronic state $O(^1D)$ (see figure 1). Ozone photolysis in the Hartley band also leads to formation of the $O(^1D)$ atom and the O_2 molecule in the first electronic excited state $O_2(a^1\Delta_g)$. The energy transfer from the electronically excited atom $O(^1D)$ to O_2 populates the second excited electronic state $b^1\Sigma^+_g$ of the oxygen molecule that, in turn, populates the $(a^1\Delta_g)$ state via collisions with atmospheric molecules. All these excited states of atomic and molecular oxygen radiate. The model describing these processes was first suggested by Mlynczak *et al.* (1993). This model considered only electronic kinetics of O_2 and O_3 photolysis, and did not take into account the vibrational excitation of the molecular electronic states.

However, from the beginning of the 1980s (e.g. Sparks *et al.* 1980, Valentini *et al.* 1987, Thelen *et al.* 1995, Matsumi and Kawasaki 2003), it has been known that O_3 photolysis products in the first singlet and ground electronic states of the O_2 molecule are also vibrationally excited ($O_2(a^1\Delta_g, v)$ and $O_2(X^3\Sigma^-_g, v)$), where v is the vibrational quantum number. As shown in Kalogerakis *et al.* (2005), energy transfer from $O(^1D)$ to O_2 leads to formation of electronically vibrationally excited molecules $O_2(b^1\Sigma^+_g, v)$, mainly $O_2(b^1\Sigma^+_g, v = 1)$. The latter gives rise to the populations of vibrational levels of the singlet electronic state $(a^1\Delta, v)$ and of the ground electronic state $(X^3\Sigma^-_g, v)$ through the fast near-resonance processes.

These processes were investigated by Yankovsky and Manuilova (2006). They developed an extended model for O_3 and O_2 photodissociation products kinetics in the

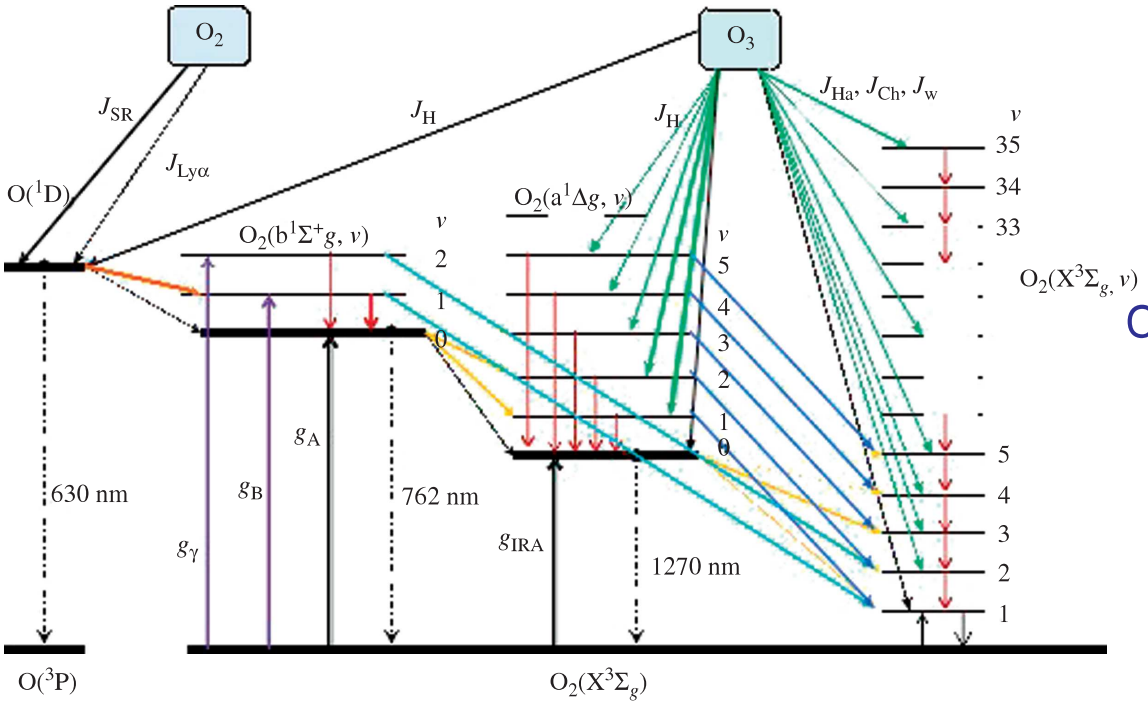

COLOUR FIGURE

Figure 1. The scheme of electronic–vibrational kinetics of the $O(^1D)$ atom, two electronic singlet excited states $O_2(b^1\Sigma_g, v = 0, 1, 2)$, $O_2(a^1\Delta_g, v = 0–5)$ and the ground electronic state $O_2(X^3\Sigma^-_g, v \leq 35)$ in the mesosphere and lower thermosphere.

MLT, hereafter known as the YM-2006 model. In the present work, we use this model for the calculations of the $O_2(X^3\Sigma^-_g, v = 1\text{–}35)$ populations.

In this work, we have focused our efforts on studying the $O_2(X^3\Sigma^-_g, v = 1)$ state population behaviour with respect to various atmospheric conditions and on the parameterization of this source of $H_2O(010)$ population, which is required for operational retrieval of H_2O volume mixing ratio (VMR) retrieval from the 6.3 μm band emission measured, in particular, by the Sounding of the Atmosphere using Broadband Emission Radiometry (SABER)/Thermosphere Ionosphere Mesosphere Energetics and Dynamics (TIMED) satellite limb infrared radiometer.

1.1 *Remote sensing of the Earth's atmosphere using the SABER instrument on board the TIMED satellite*

The TIMED satellite was launched on 7 December 2001 into a 74.1° inclined 625 km orbit with a period of 1.7 hours. The TIMED mission was focused on the energetics and dynamics of the MLT region (60–180 km) (Yee *et al.* 1999). SABER, one of four instruments on TIMED, is a 10 channel broadband limb-scanning infrared radiometer covering the spectral range from 1.27 μm to 17 μm. SABER provides vertical profiles of kinetic temperature, pressure, ozone, carbon dioxide, water vapour, atomic oxygen, atomic hydrogen and volume emission rates in the NO (5.3 μm) and OH Meinel and $O_2(a^1\Delta_g)$ bands. The vertical instantaneous field of view of the instrument is approximately 2.0 km at 60 km altitude, the vertical sampling interval is ~0.4 km, and the atmosphere is scanned from below the surface up to 400 km tangent height. The instrument performs one vertical scan every 53 s, the scans are performed both in the upwards and downwards directions. The latitudinal coverage is governed by a 60 day yaw cycle that allows observations of latitudes from 83° S to 52° N in the south viewing phase, or from 53° S to 82° N in the north viewing phase. The instrument has been performing near-continuous measurements in this mode since 25 January 2002.

1.2 *H_2O retrievals from 6.3 μm radiance measurements*

The non-equilibrium radiance in the 6.3 μm band is formed in the transitions for which the ν_2 vibrational quantum number decreases by 1:

$$H_2O(\nu_1,\nu_2,\nu_3) \rightarrow H_2O(\nu_1,\nu_2-1,\nu_3) + 6.3\,\mu\text{m}. \quad (1)$$

Correspondingly, the interpretation of this radiance requires the estimation of the $H_2O(\nu_2)$ populations, which is not a trivial task. It is well known that vibrationally excited molecular levels in the MLT and above are, in general, not in local thermodynamic equilibrium (LTE) with the surrounding media (López-Puertas and Taylor 2001).

In the lower atmosphere, the frequency of inelastic molecular collisions is sufficiently high so that these collisions dominate other population/depopulation mechanisms of the molecular vibrational levels. This leads to LTE, and the populations follow the Boltzmann distribution governed by the local kinetic temperature. In the MLT, where the frequency of inelastic collisions is much lower than that at lower altitudes, other processes (vibrational–vibrational (V–V), chemical, photochemical, radiative) also influence the populations of the vibrational levels. As a result, LTE no longer applies in this altitude region, and the populations must be found by solving

the self-consistent system of kinetic and radiative transfer equations that express the balance relations between the above-mentioned processes. This situation is called non-LTE. For $H_2O(v_2)$ levels, the LTE breaks at about 60 km altitude. Correspondingly, the interpretation of the 6.3 μm band radiance in the MLT requires the solution of the non-LTE task for a system of H_2O vibrational levels. The non-LTE model of vibrational kinetics of the H_2O molecule used in this study considers 14 vibrational levels (000, 010, 020, 100, 001, 030, 110, 011, 040, 120, 021, 200, 101, 002) up to an energy of 7000 cm^{-1} (Manuilova *et al.* 2001, Feofilov *et al.* 2009). We used HITRAN2004 database for the radiative transition parameters of the H_2O molecule involved in the calculations.

The most important process of the intermolecular V–V energy exchange in the O_2–H_2O pair is the quasi-resonance collisional energy exchange between $O_2(X^3\Sigma^-_g, v = 1)$ and vibrational levels of the v_2 mode of the H_2O molecule:

$$O_2(X^3\Sigma^-_g, v = 1) + H_2O(v_1, v_2, v_3) \leftrightarrows O_2(X^3\Sigma^-_g, v = 0) + H_2O(v_1, v_2 + 1, v_3) - \Delta E. \quad (2)$$

As will be shown below, these processes are responsible both for population and depopulation of the $H_2O(v_2)$ vibrational levels. At the 40–70 km altitude range, the first excited vibrational level $H_2O(010)$ is populated through the V–V energy exchange between $O_2(X^3\Sigma^-_g, v = 1)$ and the $H_2O(010)$ in the process:

$$O_2(X^3\Sigma^-_g, v = 1) + H_2O(000) \leftrightarrows O_2(X^3\Sigma^-_g, v = 0) + H_2O(010) - 39\ cm^{-1}, \quad (3)$$

which is a particular case of the processes in equation (2). For determination of this important source of H_2O vibrational excitation, we use the calculated altitude profile of the $O_2(X^3\Sigma^-_g, v = 1)$ concentration in the middle atmosphere. The approach and parameterization for calculating this source is explained below.

Since the calculation of $[O_2(X^3\Sigma^-_g, v = 1)]$ is a complicated task if the whole YM-2006 model is involved, we suggest a parameterization for the $O_2(X^3\Sigma^-_g, v = 1)$ population term, which can be used as an input by other models. In this paper, we name it the total Resulting Quantum Output (RQO) of $O_2(X^3\Sigma^-_g, v = 1)$ production per one act of O_3 photodissociation. We have studied the RQO behaviour for a number of test atmospheres and present the analytical formula for RQO parameterization as a function of pressure.

2. The model of electronic-vibrational kinetics of O_2 and O_3 photolysis

Figure 1 gives an overview of the electronic-vibrational kinetics processes involving the O_2/O_3 photolysis products. The scheme shows the $O(^1D)$ atom, two electronic singlet excited states of the O_2 molecule: $(b^1\Sigma^+_g, v)$, with $v = 0, 1, 2$, $(a^1\Delta_g, v)$, with $v = 0$–5, and the ground electronic state of the O_2 molecule $(X^3\Sigma^-_g, v)$, with $v = 1$–35. The energy transfer process from $O(^1D)$ to O_2 predominantly populates the first vibrational level of the second electronic state $(b^1\Sigma^+_g)$ (thick orange arrow in figure 1). Fast near-resonance reactions of electronic–electronic (E–E) exchange in the following processes:

$$O_2(b^1\Sigma^+_g, v) + O_2 \rightarrow O_2(X^3\Sigma^-_g, v) + O_2(b^1\Sigma^+_g, 0) \quad (4)$$

populate vibrational levels 1 and 2 of the ground electronic state $X^3\Sigma^-_g$ (cyan arrows in figure 1). Ozone photolysis in the Hartley band leads to vibrationally excited molecule $O_2(a^1\Delta_g, v)$ formation with v varying from 0 to 5 (green arrows in figure 1). An additional process, which populates the states $(a^1\Delta_g, v)$ with $v = 1$–3, is the collisional quenching of the $b^1\Sigma^+_g$ state (yellow arrows in figure 1). Fast near-resonance reactions of the E–E exchange:

$$O_2(a^1\Delta_g, v) + O_2 \rightarrow O_2(X^3\Sigma^-_g, v) + O_2(a^1\Delta_g, 0) \tag{5}$$

populate vibrational levels with v from 1 to 5 of the ground electronic state $X^3\Sigma^-_g$ (blue arrows in figure 1). The ozone photolysis process in the triplet channel (the Hartley, Huggins, Chappuis and Wulf bands in the spectral region from 200 to 900 nm) excites the ground electronic state $(X^3\Sigma^-_g, v)$ up to the 35th vibrational level (green arrows in figure 1):

$$O_3 + h\nu \rightarrow O_2(X^3\Sigma^-_g, v \leq 35) + O(^3P). \tag{6}$$

Vibrational levels of $O_2(X^3\Sigma^-_g, v)$ are depopulated by V–V and V–T energy exchange processes in collisions with O_2, N_2 and $O(^3P)$ (red vertical arrows in figure 1). AQ1

All these processes have been taken into account in the YM-2006 model. The populations of the states are calculated by solving the system of kinetic equations for all 45 electronic-vibrational states under consideration: the first excited state of atomic oxygen, $O(^1D)$, three states of $O_2(b^1\Sigma^+_g, v)$, six states of $O_2(a^1\Delta_g, v)$ and 35 states of $O_2(X^3\Sigma^-_g, v)$. For all these 45 states that are interrelated by photochemical reactions, a system of 45 first-order kinetic equations is solved on a regular altitude grid:

$$\frac{\partial n_i}{\partial t} \sum_{k=1,k\neq i}^{45} n_k P_i^k + \sum_l F_i^l - n_i \sum_m q_i^m, \tag{7}$$

where i is the level number ($i = 1$–45), is the population of the ith level, is the production rate of the ith component out of k components ($k = 1$–45, $k \neq i$) in the collisional processes of energy transfer, $q_i{}^m$ is the total quenching of component i in the processes of collisional and radiative quenching, and $F_i{}^l$ is the production rate for the ith component in the photolysis of O_2 and O_3 molecules (equation (7)) and in chemical reactions (e.g. in collisional reactions of O with O_3).

The system of differential equations (7) can be written as a matrix equation for the vector of the level population $\boldsymbol{n}$:

$$\frac{\partial \boldsymbol{n}}{\partial t} = \mathbf{A} \cdot \boldsymbol{n} + \boldsymbol{F} \tag{8}$$

In a stationary case, equation (7) can be written as a system of algebraic equations:

$$\boldsymbol{n} = -\mathbf{A}^{-1} \cdot \boldsymbol{F}, \tag{9}$$

where $\mathbf{A}$ is a quasi-diagonal sparse matrix. The method of solution of such systems of equations is described in Olemskoy (2006).

Summarizing, the model developed enables us to solve both the problem of calculations of the excited product concentrations and the inverse problem of ozone retrieval from intensities of emissions of electronic-vibrationally excited O_2 molecules.

3. Vibrational kinetics of $O_2(X^3\Sigma^-_g, v)$

In this update of the YM-2006 model, we have used new theoretical and experimental data for the vibrational kinetics of $O_2(X, v)$. First, we introduced into the model the new estimation of the rate constant K of the V–T quenching process:

$$O_2(X^3\Sigma^-_g, v = 1) + O_2 \rightarrow O_2 + O_2, \tag{10}$$

where $K = 1 \times 10^{-2} + 7.7 \times 10^{-11}\exp(-115/T^{1/3}) + 5.3 \times 10^{-7}\exp(-199/T^{1/3})$ (Huestis 2006). Strong dependence of this rate constant on temperature in comparison with commonly used rate constant $K = 4.2 \times 10^{-19}(T/300)^{0.5}$ (López-Puertas *et al.* 1995) leads to a 2.0–2.5 times increase of the first excited vibrational level population, $O_2(X^3\Sigma^-_g, v = 1)$, near the mesopause and to its 1.5–2.0 times decrease near the stratopause.

Second, for the most important process of vibrational relaxation of $O_2(X^3\Sigma^-_g, v)$ in collisions with $O(^3P)$:

$$O_2(X^3\Sigma^-_g, v \leq 30) + O \rightarrow O_2(X^3\Sigma^-_g, v\square = v - \Delta v) + O, \tag{11}$$

AQ4

the new model of rate constants (Esposito *et al.* 2008) was used for the first time. This model describes not only the total quenching, but also the intermolecular V–V energy exchange between upper and lower vibrational levels, when the lower vibrational levels are populated. The rate constant of this reaction strongly depends on temperature. Figure 2 shows the dependence of rate constants of these reactions on v and Δv. Detailed calculations of altitude profile $O_2(X^3\Sigma^-_g, v)$ concentrations for different vibrational levels up to $v \leq 35$ using the updated YM-2006 model were presented in Yankovsky and Babaev (2010).

López-Puertas *et al.* (1995) estimated that in the whole altitude range, the quantum yield of the vibrationally excited $O_2(X^3\Sigma^-_g, v = 1)$ per one photodissociated O_3 molecule was equal to 4. Utilizing the YM-2006 photolysis model enables us to calculate the $O_2(X^3\Sigma^-_g, v = 1)$ population precisely for any given distribution of atmospheric constituents and solar flux. We have used this model to calculate the altitude profiles of the $O_2(X^3\Sigma^-_g, v)$ vibrational level populations for a number of test cases (see figure 3). The purpose of this test was to verify the model for various solar fluxes, so we have found 12 events in mid-latitudes (from 38.9° N to 47.7° N) during the summer solstice in the northern hemisphere in 2002 that cover the solar zenith angle θ_z grid in the interval $\theta_z = 36.0°$–$90.1°$. The atmospheric conditions for these runs were taken from SABER V1.07 satellite experiment dataset available at http://saber.gats-inc.com/. The parameters of the SABER scans are listed in table 1.

We also calculated the altitude profiles of $O_2(X^3\Sigma^-_g, v = 1)$ concentration for four typical atmospheric scenarios selected for the summer solstice in the northern hemisphere: subarctic summer (SAS: 70° N; $\theta_z = 46.5°$), mid-latitude summer (MLS: 40° N; $\theta_z = 16.5°$), tropics (TROP: 0°; $\theta_z = 23.5°$) and mid-latitude winter (MLW: 40° S; $\theta_z = 63.5°$). We did not select the subarctic winter scenario since high latitudes

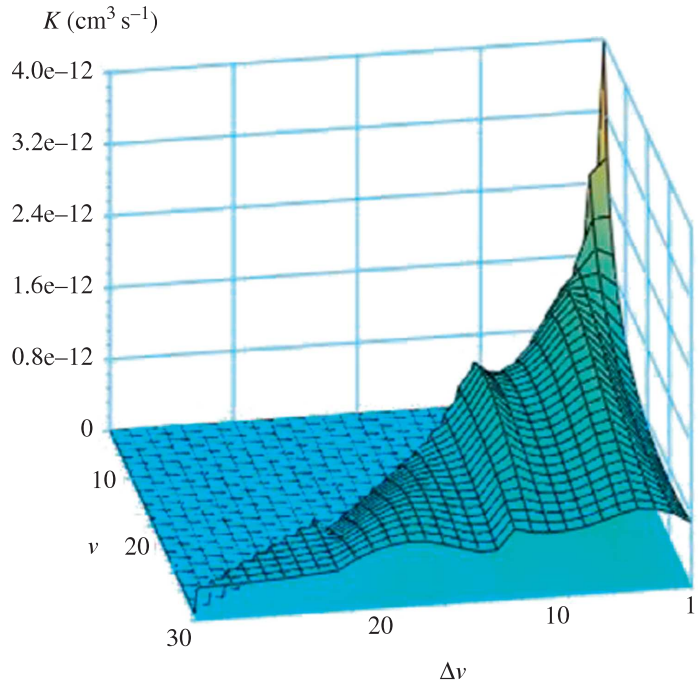

COLOUR FIGURE

Figure 2. The dependence of rate constants of reactions $O_2(X^3\Sigma^-_g, v \leq 30) + O \rightarrow O_2(X^3\Sigma^-_g, v\square = v - \Delta v) + O$ on v and Δv (Esposito *et al*. 2008) for gas temperature 200 K.

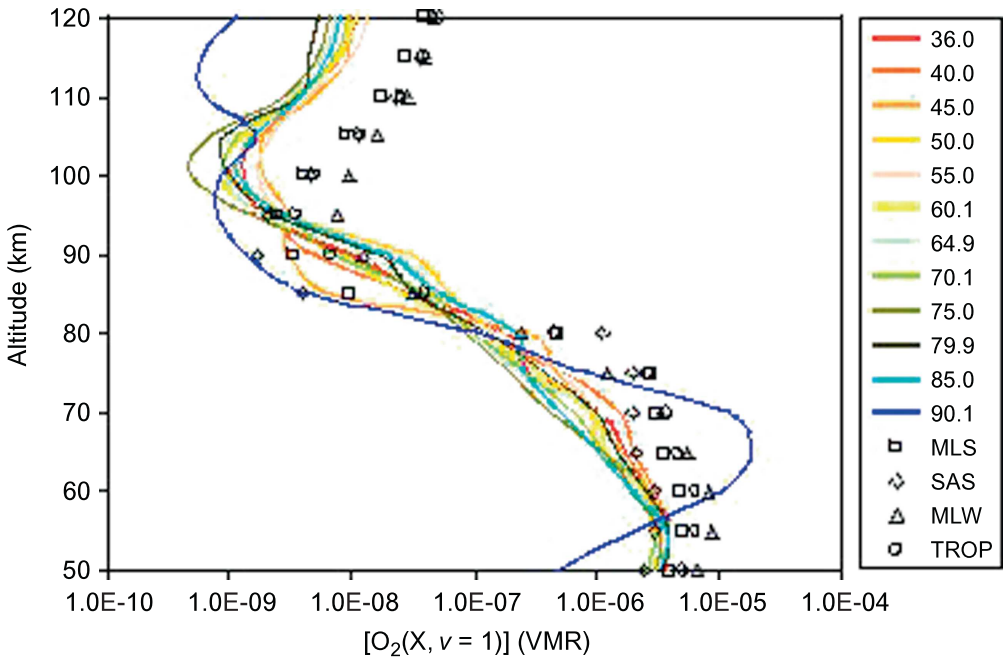

COLOUR FIGURE

Figure 3. Altitude profiles of $O_2(X^3\Sigma^-_g, v = 1)$ volume mixing ratio calculated for different atmospheric conditions: curves – SABER data (see table 1), solar zenith angles are shown in the legend; symbols – four atmospheres, (TROP: tropical; SAS: subarctical summer; MLW: mid-latitude, winter; MLS: mid-latitude summer).

in the southern hemisphere are not illuminated by the Sun during this season. The main difference between these atmospheric scenarios is the temperature profile that enables the study of the temperature-dependent effects in the model, including the

Table 1. TIMED/SABER events selected for test runs.

Event	Latitude (°)	Longitude (°)	Date	θ_z (°)
29_01305	42.2	286.6	5 March 2002	70.08
31_01378	42.7	297.2	10 March 2002	60.07
32_01218	47.7	259.9	27 February 2002	85.03
35_01238	41.1	129.1	01 March 2002	79.89
36_01278	44.4	228.7	04 March 2002	75.04
36_01468	43.3	251.1	16 March 2002	49.97
37_01337	41.2	222.1	08 March 2002	64.94
38_01176	42.6	209.1	25 February 2002	90.07
38_01408	40.9	281.7	12 March 2002	55.00
38_01491	34.2	47.0	18 March 2002	39.99
39_01480	38.9	316.7	17 March 2002	45.00
40_01498	30.2	235.5	18 March 2002	36.01

thermal radiation effects. An important consequence of temperature profile variation from model to model is the pressure difference that leads to changes in optical depths for certain altitudes, which is important for photolysis rates calculations. We have used temperature, total density, O_2 and N_2 VMR profiles obtained from the MSIS-E-90 model available online (http://omniweb.gsfc.nasa.gov/vitmo/msis_vitmo.html) for the summer solstice of 2002. The other atmospheric constituents needed for the calculations (O_3, $O(^1D)$, $O(^3P)$) were taken from the corresponding zonal averages of SABER for the same time of the year.

Figure 3 shows the altitude profiles of $O_2(X^3\Sigma^-_g,\ v=1)$ concentration for 12 SABER events listed in table 1 and for four typical atmospheric scenarios. As one can see, all the profiles are close to each other for all the cases, except for the twilight one ($\theta_z = 90.1°$). In accordance with the reaction in equation (11), the enhancement of the $O_2(X^3\Sigma^-_g,\ v=1)$ concentration below 78 km is connected with a sharp decrease of atomic oxygen abundance below this altitude at twilight.

4. Parameterization of $O_2(X^3\Sigma^-_g,\ v=1)$ production

The calculation of $O_2(X^3\Sigma^-_g,\ v=1)$ concentration using the whole YM-2006 model is a complicated task so we suggest a parameterization, namely, the total RQO of the $O_2(X^3\Sigma^-_g,\ v=1)$ production.

The RQO for the $O_2(X^3\Sigma^-_g,\ v=1)$ level production due to ozone photolysis in the Hartley, Huggins, Chappuis and Wulf bands (200–900 nm) is defined by the following expression:

$$\mathrm{RQO} = \frac{[O_2(X, v=1)]\, Q(O_2(X, v=1))}{\{J_{\mathrm{Hartley}} + J_{\mathrm{Chappuis}} + J_{\mathrm{Huggins}} + J_{\mathrm{Wulf}}\}\,[O_3]} \tag{12}$$

where $[O_2(X,\ v=1)]$ is the $O_2(X^3\Sigma^-_g,\ v=1)$ concentration calculated in accordance with the YM-2006 model without the contribution of O_2 photolysis, $Q(O_2(X,\ v=1))$ is a factor of $O_2(X^3\Sigma^-_g,\ v=1)$ quenching in collisions with N_2, O_2 and $O(^3P)$, and J_{Hartley}, J_{Chappuis}, J_{Huggins} and J_{Wulf} are the ozone photodissociation rates for the corresponding bands.

We stress here that in the RQO approach, we take into account the $O_2(X^3\Sigma^-_g, v)$ formation, not only in the direct processes of O_3 photolysis, but also in the processes of energy transfer from $O_2(b^1\Sigma^+_g, v)$ and $O_2(a^1\Delta_g, v)$ to $O_2(X^3\Sigma^-_g, v)$ (see figure 1). Figure 4 shows the RQO profiles in the MLT calculated for the same 12 test cases as in §3 (see table 1). As one can see, the altitude profiles of RQO for the 12 events of TIMER/SABER correspond to each other with a confidence interval of 3Σ. The important finding made in this study is the independence of RQO on latitude, longitude and solar zenith angle (figure 4), which enables us to tabulate it or to create a universal formula for its calculation.

We suggest the following analytic formula for RQO parameterization depending on pressure in the interval from 1 mb to 2×10^{-5} mb:

$$\mathrm{RQO} = \exp(A + B(\ln(p))^2 + Cp), \tag{13}$$

where $A = 2.1370 \pm 0.0328$, $B = -0.0366 \pm 0.00207$ and $C = -0.1099 \pm 0.0720$ are the parameterization coefficients, and p is the pressure in mb. This formula fits the RQO with the correlation coefficient $r^2 = 0.9916$ and gives a fit standard error equal to 0.2741 (see figure 4). We also tested the RQO parameterization for the four above-mentioned typical atmospheric scenarios selected for the summer solstice in the northern hemisphere. It was found that the calculated RQO profiles for these four test atmospheric models are close (within the 3Σ limits shown in figure 4) to the RQO calculated in accordance with the analytical formula of equation (13). It should be noted that the RQO parameterization is applicable for calculations of $O_2(X^3\Sigma^-_g, v = 1)$ pumping in the altitude interval 50–90 km. Above 90 km, the role of O_2 photolysis in the $O_2(X^3\Sigma^-_g, v = 1)$ formation must be taken into account and the full YM-2006 model should be used for calculations of $O_2(X^3\Sigma^-_g, v = 1)$ concentration (see figures 1 and3).

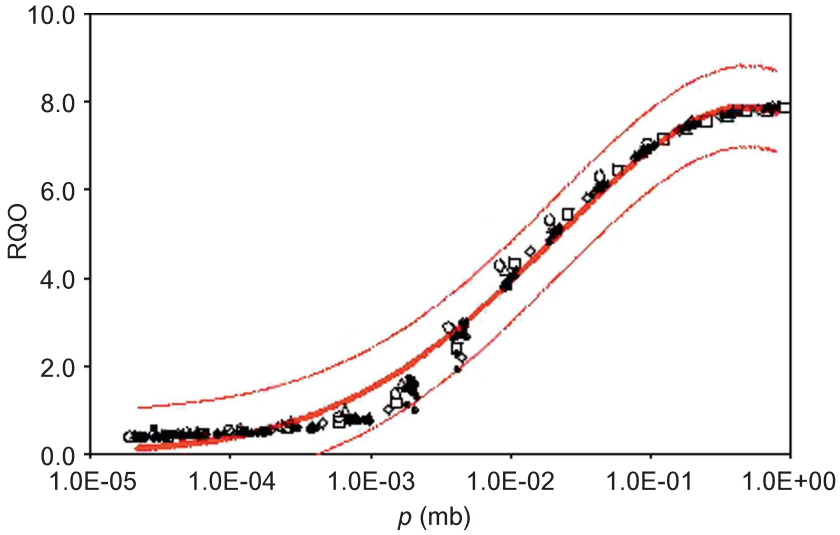

COLOUR FIGURE

Figure 4. Resulting quantum output production of $O_2(X^3\Sigma^-_g, v = 1)$ (RQO) calculated for O_3 photolysis in Hartley, Huggins, Chappuis and Wulf bands (200–900 nm) in the mesosphere and lower thermosphere. Black dots: RQO calculated for conditions of SABER data (see table 1); thick red line: RQO parameterization, equation (13); thin red lines: parameterization confidence interval 3σ; symbols: RQO calculated for four atmospheric models (MLS, SAS, MLW, TROP). Symbols for atmospheric models are the same as in figure 3.

5. Applications of RQO to H_2O retrieval in the mesosphere

We estimated the population of $H_2O(010)$ and $O_2(X^3\Sigma^-_g, v = 1)$ and tested the effects of the RQO parameterization using the Accelerated Lamda Iterations for Atmospheric Radiation and Molecular Spectra (ALI-ARMS) research code (see Kutepov *et al.* 1998, Gusev and Kutepov 2003 and references therein) that solves the non-LTE multi-level problem for an arbitrary number of molecular levels in the atmosphere by iterative solving of a set of statistical equilibrium equations and the radiative-transfer equations. For these calculations, the code was modified to include a 'source' member to the statistical equilibrium equation describing the population and depopulation of the $O_2(X^3\Sigma^-_g, v = 1)$ level. The other atmospheric components that were included to the non-LTE task are: H_2O (1 isotope, 14 vibrational levels), CO_2 (5 isotopes, 60 vibrational levels), N_2 (1 isotope, 7 vibrational levels), $O(^3P)$ and $O(^1D)$. In figure 5, we demonstrate the significance of the process (2) for the vibrational kinetics of the H_2O molecule. Figure 5 shows the ratio of H_2O (010) population calculated for the case of $H_2O(v_1, v_2, v_3)$–$O_2(X^3\Sigma^-_g, v = 1)$ V–V coupling to H_2O (010) population obtained in the case when the reaction (3) is not taken into account for the four atmospheric models.

As one can see from figure 5, below 70 km, taking into account the V–V energy exchange between $O_2(X^3\Sigma^-_g, v = 1)$ and $H_2O(010)$ (2) leads to a 2–12% increase of the $H_2O(010)$ level population. The most important influence of processes (3) on the population of 010 is connected with deactivation of vibrational levels 010, 020, 030, 110, 011, 040, 120 and 021 at near-resonance V–V energy exchange with $O_2(X^3\Sigma^-_g, v = 1)$ above 70 km, which leads to a decrease of the 010 level population from 45% to 75% at 85 km, in comparison with the population of 010 calculated without taking this process into account.

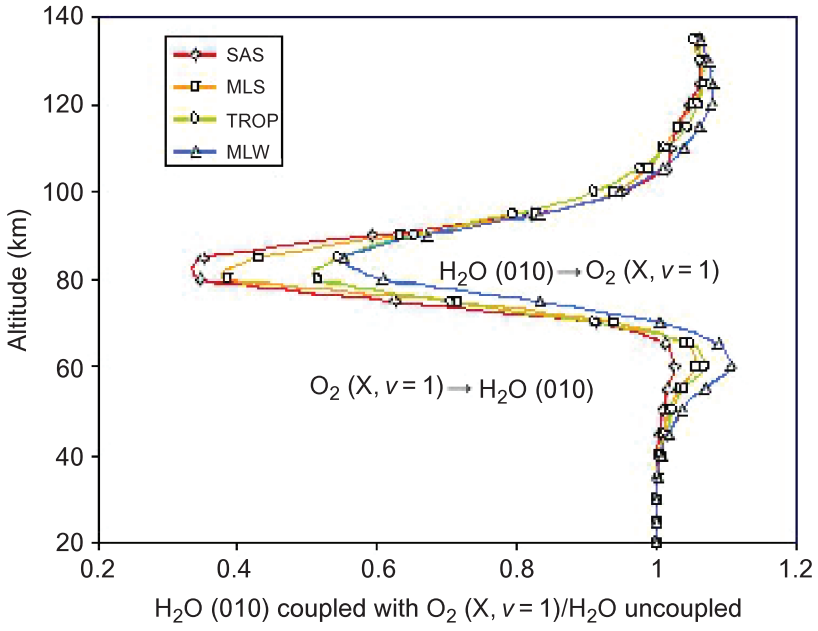

COLOUR FIGURE

Figure 5. The ratio of $H_2O(010)$ population calculated for four atmospheric models (MLS, SAS, MLW, TROP), taking into account the processes of intermolecular quasi-resonance (V–V) energy exchange between $O_2(X^3\Sigma^-_g, v = 1)$ and $H_2O(v_1, v_2, v_3)$ to $H_2O(010)$ population calculated without taking these processes into account.

First, the ALI-ARMS code was run with fixed RQO = 4 (López-Puertas *et al.* 1995, López-Puertas and Taylor 2001) for the four typical atmospheric scenarios described above. Then, the fixed RQO in the code was replaced with that defined by equation (13), and new calculations were carried out. The results are compared in figures 6 and 7. Figure 6 is in agreement with figure 5: in the lower atmosphere, the variable RQO leads to stronger pumping of the $O_2(X^3\Sigma^-_g, v = 1)$ level, while in the upper

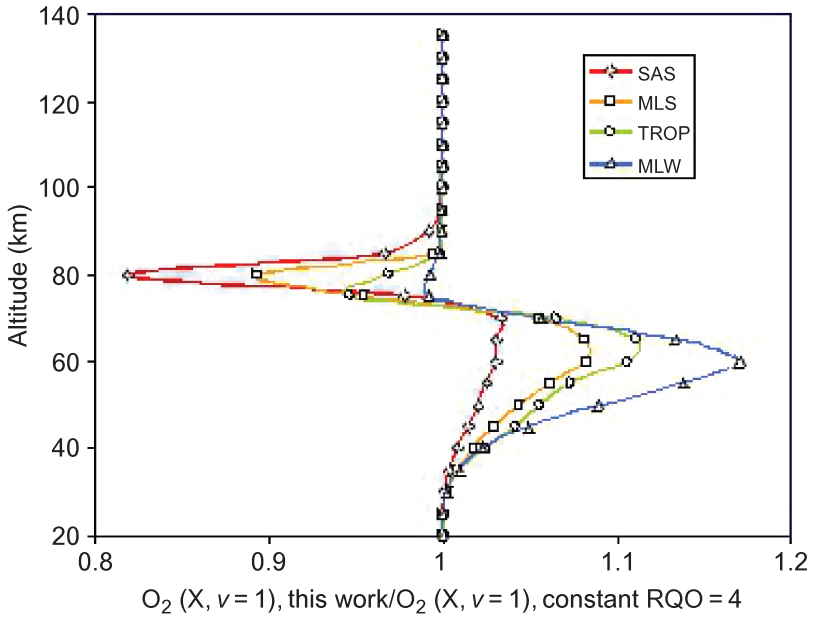

COLOUR FIGURE

Figure 6. The ratio of $O_2(X^3\Sigma^-_g, v = 1)$ population calculated for four atmospheric models (MLS, SAS, MLW, TROP) using the RQO parameterization (13) to $O_2(X^3\Sigma^-_g, v = 1)$ population calculated using fixed RQO = 4 (López-Puertas *et al*. 1995).

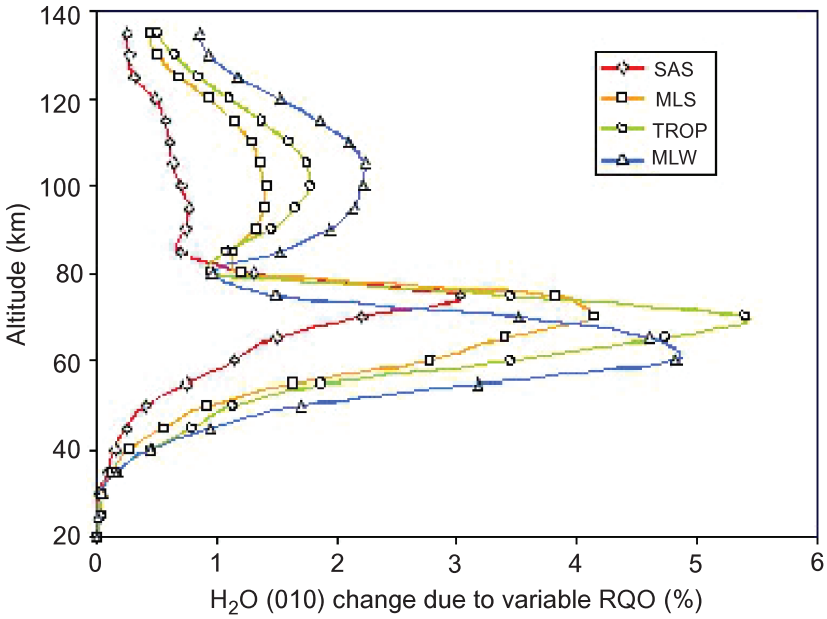

COLOUR FIGURE

Figure 7. The ratio of $H_2O(010)$ population calculated for four atmospheric models (MLS, SAS, MLW, TROP) using the RQO parameterization (equation (13)) to $H_2O(010)$ population calculated using fixed RQO = 4 (López-Puertas *et al*. 1995).

atmosphere, the $O_2(X^3\Sigma^-_g, v = 1)$ level is pumped less in comparison with the fixed RQO = 4. The behaviour of the $H_2O(010)$ in figure 7 needs commenting on. Obviously, the 3% to 5% increase in $H_2O(010)$ population at 60-70 km altitude is due to increased $O_2(X^3\Sigma^-_g, v = 1)$ pumping. However, the area above 80 km altitude also experiences an increase in the $H_2O(010)$ population, although the $O_2(X^3\Sigma^-_g, v = 1)$ is less pumped at these altitudes. The explanation lies in the non-local character of the $H_2O(010)$ populations: this extra $H_2O(010)$ pumping is due to radiative transfer from the layers below, which, as we know from figure 7, have higher populations in the case of variable RQO.

We demonstrate an example of the RQO approach application to H_2O VMR retrievals from SABER measurements (see figure 8). The retrieval methodology has been described in detail in Feofilov *et al.* (2009). Briefly, the ALI–ARMS code uses the forward-fitting technique, in which the process starts with an initial guess of the H_2O altitude profile. The non-LTE populations are calculated and used for limb-radiance calculations. The H_2O VMR is adjusted at each tangent height in accordance with the ratio of measured and calculated radiance. The iterations are repeated until the differences between the simulated and measured radiances become equal to the radiance noise in the channel. In this work, we have calculated the population term for the $O_2(X^3\Sigma^-_g, v = 1)$ level for each tangent altitude using the RQO calculated in accordance with equation (13). The interactions of the $O_2(X^3\Sigma^-_g, v = 1)$ level with other molecules and atoms (H_2O, CO_2, O) have not been changed with respect to the full non-LTE model of H_2O (López-Puertas and Taylor 2001, Manuilova *et al.* 2001, Feofilov *et al.* 2009). The retrieval has been performed for the 12 test cases from table 1. As one can see in figure 8, the absolute values of the H_2O VMR retrieved in this approach are in agreement with other measurements (Nedoluha *et al.* 2007). The error bars for the retrievals shown in figure 8 are ~10% at and below 70 km, 20%

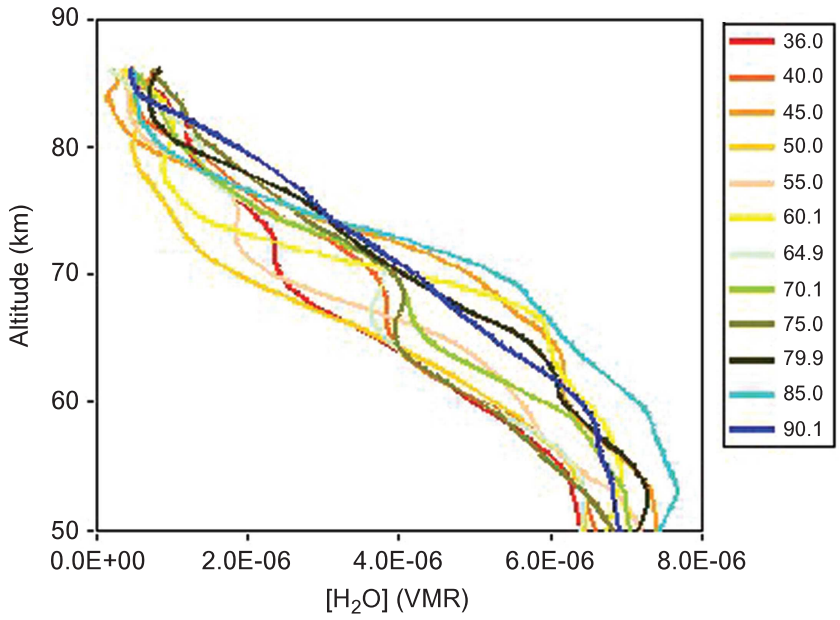

COLOUR FIGURE

Figure 8. Altitude profiles of H_2O volume mixing ratio retrieved from 6.3 μm band radiance measured by SABER (see table 1). Solar zenith angles are shown in the legend. The non-LTE model of the H_2O model used for the retrieval included 14 excited vibrational levels and the RQO parameterization formula.

at 80 km and 30% at 85 km (Feofilov *et al.* 2009). Taking into account the retrieval uncertainty and temporal and spatial variability of the water vapour, one may speculate that figure 8 shows no dependence of H_2O VMR on θ_z. This is in agreement with the long (20–30 hours) photochemical lifetime of water vapour in the altitude range considered (Brasseur and Solomon 2005). Summarizing, the RQO approach applied to H_2O VMR retrievals from SABER measurements provides reliable results at no computational cost.

6. Conclusions

We have updated the model of electronic-vibrational kinetics of the O_2 and O_3 photodissociation in the MLT by including the most recent estimate of the quenching rate of $\{O_2(X^3\Sigma^-_g,\ v = 1) + O_2\}$ and $\{O_2(X^3\Sigma^-_g,\ v \leq 30) + O\}$. The latter process is extremely important for $O_2(X^3\Sigma^-_g,\ v \leq 30)$ vibrational de-excitation, so we used a model that not only calculates the total quenching rate, but also describes the intermolecular V–V energy exchange between upper and lower vibrational levels, when the lower vibrational levels $O_2(X^3\Sigma^-_g,\ v)$ are populated. As a result, an updated YM-2006 model enables one to calculate the altitude dependence of the populations of 35 vibrational states of O_2 molecules in the ground electronic state.

We have described the RQO approach for estimating the $O_2(X^3\Sigma^-_g,\ v = 1)$ vibrational level pumping and suggested a parameterization of the RQO that can be used in the non-LTE models of trace gas molecules in the MLT. The RQO describes the net effect of the $O_2(X\ ^3\Sigma^-_g,\ v = 1)$ level production due to ozone photolysis in the Hartley, Huggins, Chappuis and Wulf bands (200–900 nm). We have studied the RQO behaviour in the latitude interval from 70° N to 70° S and for θ_z up to 90° with respect to different atmospheric conditions, and found that it depends strongly on altitude, and weakly on the solar zenith angle, latitude, longitude and season.

We have demonstrated RQO approach applications to H_2O VMR retrievals from 6.3 μm SABER radiometric measurements. The RQO approach has been incorporated into the H_2O non-LTE model in the SABER operational code, and will be used for H_2O retrievals in the next release of SABER data.

Acknowledgements

We are grateful to Dr Fabrizio Esposito and his colleagues from the Istituto di Metodologie Inorganiche e dei Plasmi, Bari, Italy for providing the code of calculation of reaction (11) rate constant. The study was supported by grant RFBR no. 09-05-00 694-a.

References

Brasseur, G.P. and Solomon S.C., 2005, *Aeronomy of the Middle Atmosphere* (Dordrecht, The Netherlands: Springer).

Esposito, F., Armehise, I., Capitta, G. and Capitelli, M., 2008, O–O_2 state-to-state vibrational relaxation and dissociation rates based on quasiclassical calculations. *Chemical Physics*, **351**, pp. 91–98.

Feofilov, A.G., Kutepov, A.A., Pesnell, W.D., Goldberg, R.A., Marshall, B.T., Gordley, L.L., García–Comas, M., López-puertas, M., Manuilova, R.O., Yankovsky, V.A., Petelina, S.V. and Russell III, J.M., 2009, Daytime SABER/TIMED observations of water vapor in the mesosphere: retrieval approach and first results. *Atmospheric Chemistry and Physics*, **9**, pp. 8139–8158.

Gusev, O.A. and Kutepov, A.A., 2003, Non-LTE gas in planetary atmospheres. In *Stellar Atmosphere Modeling*, I. Hubeny, D. Mihalas and K. Werner (Eds), *ASP Conference Series*, vol. 288, pp. 318–330.

Huestis, D.L., 2006, Vibrational energy transfer and relaxation of O_2 and $H_2O^{\#}$. *Journal of Physical Chemistry A*, **110**, pp. 6638–6642.

Kalogerakis, K.S., Pejakovic, D.A., Copeland, R.A. and Slanger, T.G., 2005, Relative yield of $O_2(b^1\Sigma^+_g, v = 0$ and 1) in $O(^1D) + O_2$ collisions. *EOS Transactions AGU*, **86(52)**, *AGU Fall Meeting*, SA11A-0220, San Francisco, CA, 5–9 December 2005.

Kutepov, A.A., Gusev, O.A. and Ogibalov, V.P., 1998, Solution of the non-LTE problem for molecular gas in planetary atmospheres: superiority of accelerated lambda iteration. *Journal of Quantitative Spectroscopy and Radiative Transfer*, **60**, pp. 199–220.

López-puertas, M. and Taylor, F.W., 2001, *Non-LTE Radiative Transfer in the Atmosphere* (River Edge, NJ: World Scientific Publishing Co.).

López-puertas, M., Zaragoza G., Kerridge, B.J. and Taylor, F.W., 1995, Non-local thermodynamic equilibrium model for H_2O 6.3 and 2.7 μm bands in the middle atmosphere. *Journal of Geophysical Research*, **D100**, pp. 9131–9147.

Manuilova, R.O., Yankovsky, V.A., Gusev, O.A., Kutepov, A.A., Sulakshina, O.N. and Borkov, YU.G., 2001, Non-equilibrium middle atmosphere radiation in the infrared ro-vibrational water vapor bands. *Atmospheric and Oceanic Optics*, **14**, pp. 864–867.

Matsumi, Y. and Kawasaki, M., 2003, Photolysis of atmospheric ozone in the ultraviolet region. *Chemical Reviews*, **103**, pp. 4767–4781

Mlynczak, M.G., Solomon, S.C. and Zaras, D.S., 1993, An updated model for $O_2(a^1\Delta_g)$ concentrations in the mesosphere and lower mesosphere and implications for remote sensing of ozone at 1.27 μm. *Journal of Geophysical Research*, **D98**, pp. 18 639–18 648.

Nedoluha, G.E., Gomez, R.M., Hicks, B.C., Bevilacqua, R.M., Russell III, J.M., Connor, B.J. and Lambert, A., 2007, A comparison of middle atmospheric water vapor as measured by WVMS, EOS–MLS, and HALOE. *Journal of Geophysical Research*, **112**, D24S39, doi: 10.1029/2007JD008757.

Olemskoy, I.V., 2006, Updating of algorithm of allocation structural features. *Vestnnik Sankt-Peterburgskogo Universiteta. Seriya 10: Prikladnaya. Matemematika*, **1**, pp. 55–64.

Sonnemann, G. R., Grygalashvyly, M. and Berger, U., 2005, Autocatalytic water vapor production as a source of large mixing ratios within the middle to upper mesosphere. *Journal of Geophysical Research*, **110**, D15303, doi: 10.1029/2004JD005593.

Sparks, R.K., Carlson, L.R., Snobatake, K., Kowalczyk, M.L. and Lee, Y.T., 1980, Ozone photolysis: a determination of the electronic and vibrational state distributions of primary products. *Journal of Chemical Physics*, **72**, pp. 1401–1402.

Thelen, M.A., Gejo, T., Harrison, J.A. and Huber, J.R., 1995, Photodissociation of ozone in the Hartley band: fluctuation of the vibrational state distribution in the $O_2(a^1\Delta_g, v)$ fragment. *Journal of Chemical Physics* **103**, pp. 7946–7955.

Valentini, J.J., Gerrity, D.P., Phillips, D.L., Nieh, J.-C. and Tabor, K.D., 1987, CARS spectroscopy of $O_2(a^1\Delta_g)$ from the Hartley band photodissociation of O_3: dynamics of the dissociation. *Journal of Chemical Physics*, **86**, pp. 6745–6756.

Yankovsky, V.A. and Babaev, A.S., 2010, Photolysis of O_3 in the Hartley, Huggins, Chappuis and Wulf bands in the middle atmosphere: vibrational kinetics of oxygen molecules $O_2(X^3\Sigma^-_g, v \leq 35)$. *Atmospheric and Oceanic Optics*, **23**, pp. 640–649.

Yankovsky, V.A. and Manuilova, R.O., 2006, Model of daytime emissions of electronically vibrationally excited products of O_3 and O_2 photolysis: application to ozone retrieval. *Annales Geophysicae*, **24**, pp. 2823–2839. AQ3

Yankovsky, V.A., Kuleshova, V.A., Manuilova, R.O. and Semenov, A.O., 2007, Retrieval of total ozone in the mesosphere with a new model of electronic vibrational kinetics of O_3 and O_2 photolysis products. *Atmospheric and Oceanic Physics*, **43**, pp. 514–525.

Yee, J.-H., Cameron, G.E. and Kusnierkiewicz, D.Y., 1999, Overview of TIMED. *SPIE*, **3756**, pp. 244–254.